Infrared Spectra of $M(OH)_{1,2,3}$ (M = Mn, Fe, Co, Ni) Molecules in Solid Argon and the Character of First Row Transition Metal Hydroxide Bonding

Xuefeng Wang and Lester Andrews*

Chemistry Department, University of Virginia, P.O. Box 400319, Charlottesville, Virginia 22904-4319

Received: April 21, 2006; In Final Form: June 12, 2006

Reactions of laser-ablated Mn, Fe, Co, and Ni atoms with H_2O_2 and with $H_2 + O_2$ mixtures in excess argon give new absorptions in the O−H and M−O stretching regions, which are assigned to metal dihydroxide and trihydroxide molecules, $M(OH)_2$ and $M(OH)_3$. Isotopic substitutions (D_2O_2, $^{18}O_2$, $^{16,18}O_2$, D_2) confirmed the assignments and DFT calculations reproduced the experimental results. The O−H stretching frequencies decreased in the dihydroxides from Sc to Zn. Mulliken and natural charge distributions indicate significant electron transfer from metal d orbitals to OH ligands that decreases from Sc to Zn, suggesting that the early transition metal hydroxides are more ionic and that the later transition metal hydroxides are more covalent.

Introduction

Alkali and heavy alkaline earth metal hydroxides are strong bases in aqueous solution, but pure transition metal hydroxides are more or less insoluble.[1,2] Transition metal hydroxides from Group 3 trihydroxides to Groups 7−12 dihydroxides are known as solid compounds, and crystal structures have been determined for a number of simple $M(OH)_2$ solids (M = Mn, Fe, Co, and Ni).[2−4] The crystal structure and vibrational spectroscopy of $Co(OH)_2$ have been recorded,[5] and a number of important applications for this material have been found including an additive to improve the electrochemical activity of alkaline secondary batteries as electrochromic films and as nanoplatelets.[6−8] In addition, NiOH is used as an additive to increase the discharge capacity of Cd electrodes.[9] Oxy-hydroxides (MO)(OH) and various complexes for many of these metals have also been prepared.[2] In addition, metal hydroxy complex sulfates and hydrates such as $M_3(OH)_2(SO_4)_2(H_2O)_2$ (M = Mn, Co, Ni) are known as bulk materials.[10] Although such mixed transition metal hydroxide salts are widely used in heterogeneous catalysis,[11] the knowledge of bonding and spectroscopy for these complicated hydroxides is limited. Therefore, investigation of molecular properties of pure metal hydroxides is very important for fundamental understanding of their bonding and reaction mechanisms.

Molecular transition metal hydroxides have received limited study in the gas phase where CuOH is the only first row transition metal hydroxide molecule that has been studied by optical spectroscopy,[12−14] and very recently, the thermochemistry of FeOH and $Fe(OH)_2$ neutrals and cations has been investigated by mass spectroscopy.[15] However, a number of transition metal hydroxide molecules has been explored in solid matrixes from metal atom reactions with H_2O by Fudan and Rice groups.[16] Very recently, we have demonstrated that Group 3, 4, 11, and 12 $M(OH)_2$ molecules can be formed by the reaction of excited metal atoms with H_2O_2 or with $H_2 + O_2$ mixtures in excess argon and investigated by matrix IR spectroscopy.[17−20] The ionic bonding character for $Hf(OH)_2$ and $Hf(OH)_4$, which are similar to Group 2 metal dihydroxides, and covalent bonding character for $Au(OH)_2$ show the trend of transition metal hydroxide basicity decreasing from left to right in the periodic table.[18,19]

In this paper, the reactions of Mn, Fe, Co, and Ni with $O_2 + H_2$ or with H_2O_2 are investigated. Infrared spectra are used to collect molecular vibrational information, and the experimental data are reproduced by theoretical calculations. The nature of bonding is discussed for first row transition metal dihydroxide molecules based on the Mulliken and natural charge distribution and the electronic population analysis.

Experimental and Computational Methods

Laser-ablated Mn, Fe, Co, and Ni atom reactions with oxygen and hydrogen molecules in excess argon at 10 K have been described in our previous papers.[17−23] The Nd:YAG laser fundamental (1064 nm, 10 Hz repetition rate with 10 ns pulse width) was focused onto a rotating metal target (Johnson Matthey), which gave a bright plume spreading uniformly to the cold CsI window. The metal targets were polished to remove the oxide coating and immediately placed in the vacuum chamber. The laser energy was varied about 10−20 mJ/pulse. FTIR spectra were recorded at 0.5 cm^{-1} resolution on Nicolet 750 with 0.1 cm^{-1} accuracy using an MCTB detector. Matrix samples were annealed at different temperatures, and selected samples were subjected to irradiation by a medium-pressure mercury arc lamp (Philips, 175W) with the globe removed.

Urea hydrogen peroxide (UHP) (Aldrich, 98%) was used as the H_2O_2 source. At room temperature, UHP was put in a glass tube, and argon gas was passed over the sample to entrain H_2O_2 and give concentrations estimated at 0.1−0.2% based on comparison of H_2O_2 band intensities with previous work.[24,25] Deuterated urea−D_2O_2 was prepared adapting the method described by Pettersson et al.[24,25] Samples of H_2, D_2, HD, O_2, $^{18}O_2$, and $^{16,18}O_2$ were used as received to prepare argon gas mixtures of 6% in hydrogen and 0.2% in oxygen.

Complementary DFT calculations were performed using the Gaussian 98 program, the B3LYP density functional, and the 6-311++G(3df,3pd) basis set for all atoms.[26−28] All of the geometrical parameters were fully optimized, and the harmonic vibrational frequencies were obtained analytically at the optimized structures. Unscaled B3LYP frequencies provide a good

* Corresponding author. Email: lsa@virginia.edu.

10.1021/jp0624698 CCC: $33.50
Published on Web 07/29/2006

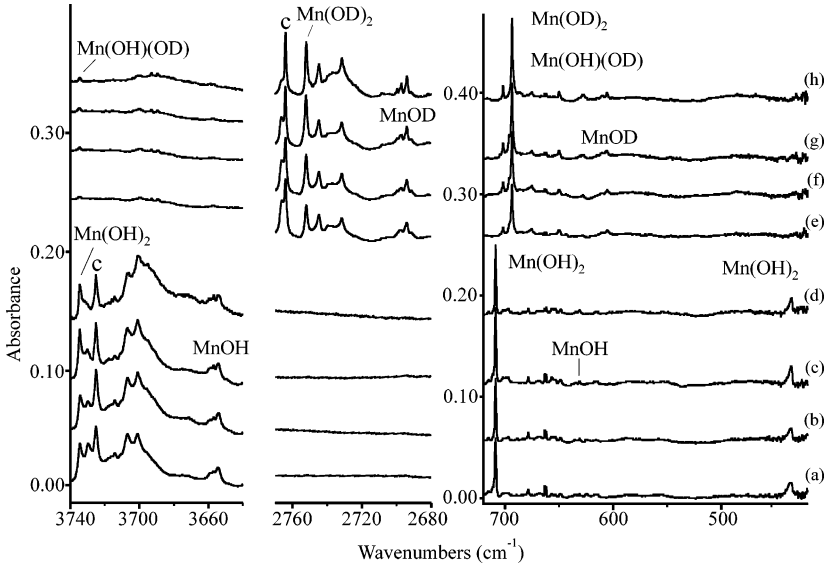

Figure 1. Infrared spectra for the manganese atom and H_2O_2 reaction products in solid argon at 10 K. (a) Mn + H_2O_2 deposition for 60 min, (b) after annealing to 20 K, (c) after >220 nm irradiation, (d) after annealing to 26 K, (e) Mn + D_2O_2 deposition for 60 min, (f) after annealing to 22 K, (g) after >220 nm irradiation, and (h) after annealing to 26 K.

approximation for observed frequencies, and accordingly, these calculations help to identify new molecules. Bonding characters were studied by natural bond orbital (NBO) analysis using Gaussian NBO Version 3.1 in the Gaussian 98 program.[26]

Results and Discussion

Infrared spectra of products formed in the reactions of laser-ablated Mn, Fe, Co, and Ni atoms with H_2O_2 or H_2 and O_2 in excess argon during condensation at 10 K will be presented. Theoretical calculations were performed to support the identifications of new metal hydroxides. These molecules have close-to-linear O−M−O bond angles and a range of M−O−H bond angles. Common species generated in the laser-ablation process and trapped in solid argon, such as O_3, O_4^-, HO_2, the OH−H_2O complex, Ar_nH^+, DO_2, the OD-D_2O complex, and Ar_nD^+, have been discussed in previous papers.[29−32] The binary metal oxides are also produced in these experiments, and these have been assigned in previous reports.[33−36]

$Mn(OH)_2$. Laser-ablated Mn atoms were co-condensed with H_2O_2 in an argon stream onto a 10 K CsI window, and additional ultraviolet irradiation and annealing were performed step-by-step. Figure 1 illustrates IR spectra for this sample so prepared. A strong, sharp band at 708.9 cm^{-1}, a weaker broad band at 435.4 cm^{-1}, and an upper band at 3734.6 cm^{-1} (labeled Mn-$(OH)_2$) appeared on deposition, increased together on ultraviolet irradiation, and decreased on further annealing. The bands at 3730, 3725.3, 3633, and 3630.1 cm^{-1} are common to laser-ablation experiments with H_2O_2 and are due to the HOH−O complex (labeled c).[17−20,25] In addition, weak bands at 948.0 and 816.4 cm^{-1} (MnO_2), 833.1 cm^{-1} (MnO), and 884.9 cm^{-1} (HMnOMnOH) were also observed.[16d,33] An analogous experiment with D_2O_2 gave a lower band at 693.6 cm^{-1} with a 701.9 cm^{-1} mixed H/D satellite and upper band at 2752.2 cm^{-1}. Unfortunately, the still lower band shifted out of our measurement range (below 400 cm^{-1}). As expected, weak MnO_2 and MnO bands appeared the same as observed in the H_2O_2 experiment, but the DMnOMnOD band shifted to 884.6 cm^{-1}.

Complementary experiments were done with $H_2 + O_2$ as the reagent to introduce ^{18}O into the subject molecule and to determine the number of oxygen atoms involved in the metal−oxygen vibrations. As shown in Figure 2, after deposition, two very weak bands at 709.6 and 435.4 cm^{-1} in the lower region and 3735.2 cm^{-1} in the upper region appeared, which increased 4-fold on 240−380 nm irradiation, and the intensities further doubled on >220 nm irradiation. These bands are essentially identical to the $Mn(OH)_2$ bands observed with H_2O_2. The bands at 948.0 and 816.4 cm^{-1} due to MnO_2 and 1592.3 cm^{-1} due to MnH_2 were observed as well, and the 884.9 cm^{-1} band was much stronger with a weak HMnOH band at 648.6 cm^{-1}. In the $^{18}O_2 + H_2$ experiment, the lower bands shifted to 687.9 and 432.2 cm^{-1}, and the upper band shifted to 3723.3 cm^{-1}, which gives the 16:18 isotopic frequency ratios 1.3155, 1.0074, and 1.0032, respectively, and shows that the 709.6 cm^{-1} band is due to an Mn−O stretching mode, 435.4 cm^{-1} is a Mn−O−H bending mode, and the 3735.2 cm^{-1} band is due to an O−H stretching mode. Reaction with H_2 and $^{16}O_2 + {}^{16}O^{18}O + {}^{18}O_2$ (1:2:1) gave the diagnostic triplet pattern at 709.6, 699.7, and 687.9 cm^{-1} for the Mn−O stretching mode, which shows that two equivalent oxygen atoms are involved. The new doublet at 3735.0 and 3723.3 cm^{-1} is very close to the O−H and ^{18}O−H stretching frequencies observed in pure isotopic experiments, suggesting that two OH subunits are barely coupled in the stretching vibrations. A broad band centered at 434.1 cm^{-1} is due to the Mn−O−H bending mode, but unfortunately, the isotopic pattern is not resolved.

With $D_2 + O_2$, the Mn−O and O−D stretching modes of the $Mn(OD)_2$ molecule were observed at 693.2 and 2752.3 cm^{-1}, respectively. The latter H/D ratio, 3735.2:2752.3 = 1.3569, is very close to the ratios found for Groups 4 and 12 metal dihydroxide molecules. With D_2 and $^{18}O_2$, the bands shift further to 671.5 and 2735.3 cm^{-1} and define slightly different 16:18 ratios, 1.0323 and 1.0062, than found for hydrogen.

The identification of $Mn(OH)_2$ is supported by DFT calculations, and the calculated unscaled frequencies are listed in Table 1. The molecular structure is converged to C_2 symmetry with the linear O−Mn−O and bent Mn−O−H subunits and ^6A ground state that is consistent with sextet ground states for the MnX_2 (X = F, Cl, Br, I) molecules.[37] The strong predicted b symmetry Mn−O stretching frequency at 729.0 cm^{-1} and O−H bending mode at 456.0 cm^{-1} are higher by 2.7 and 4.5% than the values observed at 709.6 and 435.4 cm^{-1}, which is the

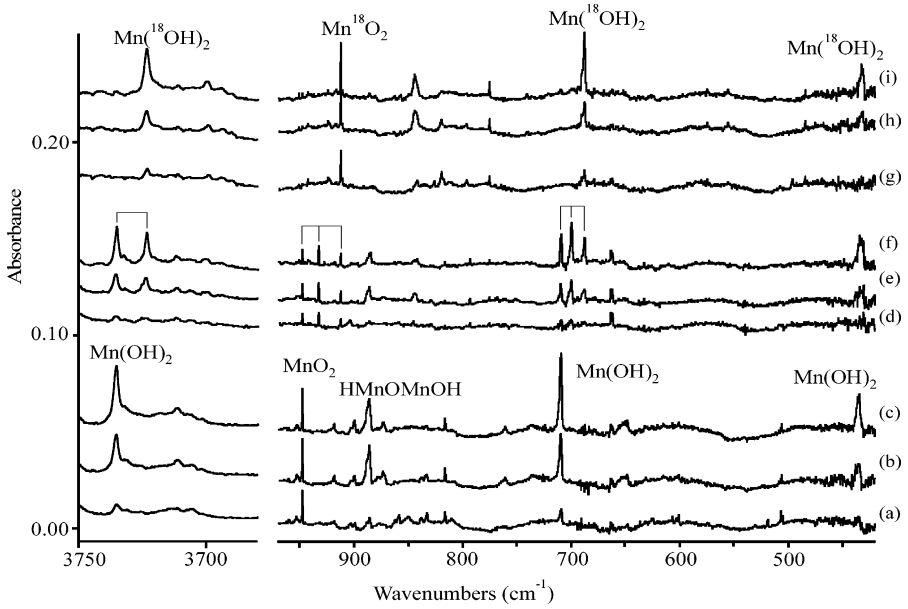

Figure 2. Infrared spectra for the manganese atom reaction products with an oxygen and hydrogen mixture in solid argon at 10 K. (a) Mn + 0.5% O_2 + 5% H_2 deposition for 60 min, (b) after >240 nm irradiation, (c) after >220 nm irradiation, (d) Mn + 0.15% $^{16}O_2$ + 0.3% $^{16,18}O_2$ + 0.15% $^{18}O_2$ + 5% H_2 deposition for 60 min, (e) after >240 nm irradiation, (f) after >220 nm irradiation, (g) Mn + 0.5% $^{18}O_2$ + 5% H_2 deposition for 60 min, (g) after >240 nm irradiation, and (h) after >220 nm irradiation.

TABLE 1: Observed and Calculated Frequencies (cm^{-1}) for $Mn(OH)_2$ (^6A in C_2 Symmetry)[a]

	$Mn(OH)_2$		$Mn(OD)_2$		$Mn(^{18}OH)_2$		$Mn(^{18}OD)_2$	
mode[b]	obsd	calcd	obsd	calcd	obsd	calcd	obsd	calcd
OH str (a)		3923.7(11)		2858.3(7)		3910.6(11)		2839.9(7)
OH str (b)	3735.2	3923.3(141)	2752.3	2857.5(106)	3723.3	3910.3(135)	2735.3	2839.2(97)
MnO str (b)	709.6	729.0(223)	693.2	714.1(273)	687.9[c]	706.6(196)	671.5	691.8(250)
MnO str (a)		606.8(2)		584.3(0)		579.1(4)		553.6(0)
MnOH bend (a)		474.1(45)		359.3(33)		466.9(42)		355.4(32)
MnOH bend (b)	435.4	456.0(240)		343.6(122)	432.2	451.9(242)		339.7(121)
MnOH bend (a)		149.4(84)		112.1(61)		148.9(81)		109.0(71)
MnOH bend (b)		117.1(4)		108.4(12)		114.3(4)		107.1(1)
OMnO bend (a)		114.4(30)		107.9(14)		110.7(30)		105.9(11)

[a] Observed frequencies from $H_2 + O_2$ experiments. Calculated at the B3LYP/6-311++G(3df,3pd)/all electron level of theory. [b] Mode descriptions and symmetries. [c] Triplet pattern at 709.6, 699.7, and 687.9 cm^{-1} was observed for this mode in reaction with H_2 and $^{16}O_2 + {}^{16}O^{18}O + {}^{18}O_2$ (1:2:1).

expected range of agreement for the B3LYP density functional.[17−20] The strong calculated b symmetry O−H antisymmetric stretching mode at 3923.3 cm^{-1} is overestimated by 5.1%, which is consistent with the predictions for other metal hydroxides.[17−20,38]

The $Mn(OH)_2$ molecule was first identified from Mn atom reactions with H_2O in solid argon, where only the strong Mn−O stretching mode of $Mn(OH)_2$ was assigned and the weaker important diagnostic O−H stretching and O−H bending modes for this molecule were not observed.[16d] In our new experiment with H_2O_2, these modes are clearly identified. Note that with H_2O_2 our 708.9 cm^{-1} $Mn(OH)_2$ band is 15 times stronger than the 884.9 cm^{-1} HMnOMnOH band, which shows that the Mn atom concentration in our experiments is relatively low and that the single metal atom species are strongly favored.

$Fe(OH)_2$. Two infrared absorptions at 3727.9 and 737.3 cm^{-1} from Fe + H_2O_2 reactions track together on deposition, irradiation, and annealing, as shown in Figure 3. The 737.3 cm^{-1} band is very sharp and reveals a completely resolved 742.3 cm^{-1} satellite with 6% of the intensity of the stronger band, which is appropriate for ^{54}Fe in natural abundance.[34] These two iron isotopic absorptions confirm that a single Fe atom is involved in this vibrational mode and product molecule. The sharp 737.3 cm^{-1} absorption was observed in Fe + H_2O experiments and assigned to $Fe(OH)_2$ based on isotopic shifts and multiplets.[16c] However, due to overlapping of the strong H_2O absorptions in the 3700−3800 cm^{-1} region, the O−H stretching mode for this molecule was not assigned. In our H_2O_2 experiments, impurity H_2O contamination was minimized, and the O−H stretching frequency appeared at 3727.9 cm^{-1}. The O−D stretching mode at 2747.5 cm^{-1} and Fe−O stretching mode at 723.8 cm^{-1} were observed with Fe + D_2O_2. In addition, the small amount of HDO_2 contamination gave the Fe(OH)(OD) molecule absorptions at 3782.2 and 731.0 cm^{-1}. As discussed previously,[16c] the three 737.3, 731.0, and 723.8 cm^{-1} bands with mixed H/D precursors show that two equivalent H(D) atoms are involved slightly in this mostly Fe−O vibrational mode. For the O−H stretching mode, the isotopic ratio H/D = 1.3568 is in line with the same mode for other transition metal hydroxides.[17−20] The Fe−O stretching mode of $Fe(OD)_2$ is again identical with that from the Fe reaction with D_2O in solid argon.[16c]

The absorptions of $Fe(OH)_2$ were also observed in the Fe atom reaction with $H_2 + O_2$ as the reagent, and the spectra are shown in Figure 4. After full-arc irradiation and annealing, the product bands increased markedly. The triplet for the Fe−O stretching mode (737.3, 727.1, and 714.5 cm^{-1}) and doublet for the O−H stretching mode (3727.9 and 3716.7 cm^{-1}) confirm the assignment.

The $Fe(OH)_2$ molecule is calculated to have a quintet ground state and C_2 symmetry with a linear O−Fe−O linkage, which

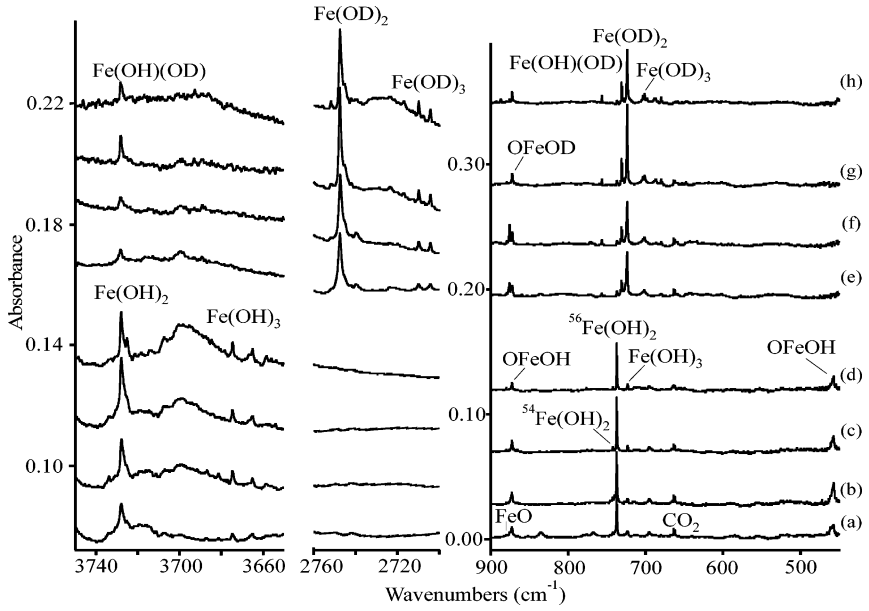

Figure 3. Infrared spectra for the iron atom and H_2O_2 reaction products in solid argon at 10 K. (a) Fe + H_2O_2 deposition for 60 min, (b) after annealing to 24 K, (c) after 240−380 nm irradiation, (d) after annealing to 30 K, (e) Fe + D_2O_2 deposition for 60 min, (f) after annealing to 20 K, (g) after 240−380 nm irradiation, and (h) after annealing to 26 K.

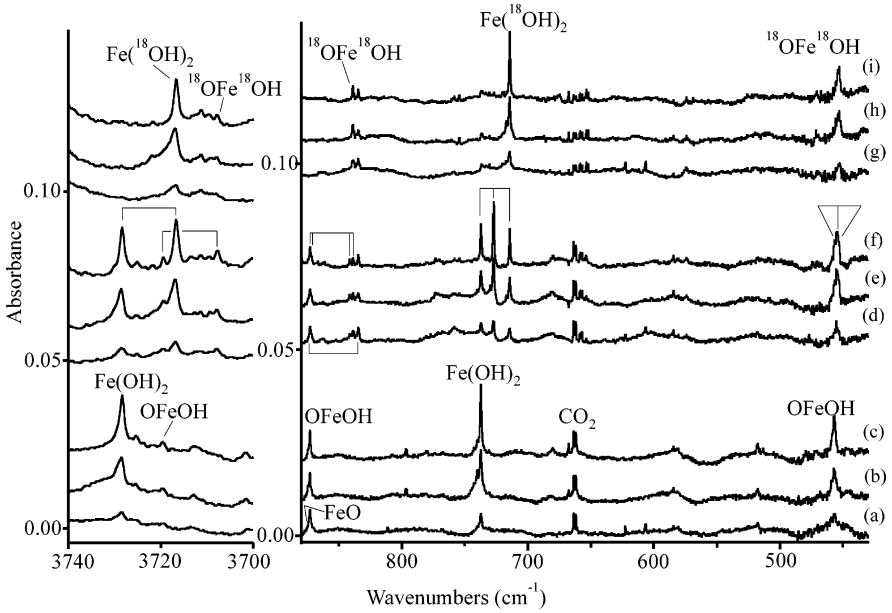

Figure 4. Infrared spectra for the iron atom reaction products with an oxygen and hydrogen mixture in solid argon at 10 K. (a) Fe + 0.5% O_2 +5% H_2 deposition for 60 min, (b) after >220 nm irradiation, (c) after annealing to 18 K, (d) Fe + 0.15% $^{16}O_2$ + 0.3% $^{16,18}O_2$ + 0.15% $^{18}O_2$ + 5% H_2 deposition for 60 min, (e) after >220 nm irradiation, (f) after annealing to 20 K, (g) Fe + 0.5% $^{18}O_2$ +5% H_2 deposition for 60 min, (g) after >220 nm irradiation, and (h) after annealing to 18 K.

is in agreement with theoretical and experimental results of iron dihalides and early theoretical calculations of $Fe(OH)_2$.[37,39] The predicted frequencies match the experimental values very well (Table 2) considering that we are comparing unscaled calculated harmonic and observed anharmonic frequencies. In addition, the antisymmetric (b symmetry) O−Fe−O stretching mode for Fe(OH)(OD) is predicted 1.0 cm^{-1} above the median for pure H and D, it is observed 0.6 cm^{-1} above, and the symmetric O−H stretching mode is predicted 1.6 cm^{-1} higher than the antisymmetric mode such that the O−H stretching mode in Fe(OH)(OD) is calculated to be 0.8 cm^{-1} higher than the strong mode for $Fe(OH)_2$, and here it is observed 0.3 cm^{-1} higher. The two new fundamental frequencies and new isotopic data presented here confirm the identification of the $Fe(OH)_2$ molecule in solid argon.

One more isotopic comparison is worth making. The iron 54:56 isotopic frequency ratio, 742.3:737.3 = 1.00678, is larger than this ratio for the FeO and FeO_2 molecules,[34] which means that more iron motion is involved in this antisymmetric vibrational mode in $Fe(OH)_2$. Correspondingly, the oxygen 16:18 isotopic frequency ratio, 737.3:714.5 = 1.0319 from the Fudan work,[16c] is less than the 16:18 ratios for the previous iron oxides, which means that less oxygen motion is involved here. These isotopic frequency ratios require that $Fe(OH)_2$ be more nearly linear at the metal center than FeO_2, and the latter was predicted to have an O−Fe−O angle of 150 ± 10°. Hence, the isotopic frequency data for the strong antisymmetric O−Fe−O stretching mode at 737.3 cm^{-1} argue for a nearly linear iron dihydroxide metal center.

TABLE 2: Observed and Calculated Frequencies (cm^{-1}) for $Fe(OH)_2$ (^5A in C_2 Symmetry)[a]

	$^{56}Fe(OH)_2$		$^{56}Fe(^{18}OH)_2$		$Fe(OD)_2$		$^{54}Fe(OH)_2$	
mode[b]	obsd	calcd	obsd	calcd	obsd	calcd	obsd	calcd
OH str (a)		3930.6(0)		3917.3(0)		2864.6(0)		3960.6(0)
OH str (b)	3727.9	3929.0(229)	3716.7	3915.9(221)	2747.5	2862.7(157)	3727.9	3929.0(221)
FeO str (b)	737.3	792.2(172)	714.5[c]	768.1(151)	723.8	771.1(221)	742.3	797.6(151)
FeO str (a)		645.5(0)		616.8(0)		612.3(0)		645.5(0)
FeOH bend (b)		428.7(307)		423.6(304)		333.1(168)		428.4(304)
FeOH bend (a)		421.7(0)		414.8(0)		322.3(0)		421.7(0)
FeOH bend (a)		216.5(137)		211.5(135)		191.3(83)		215.9(135)
FeOH bend (b)		114.8(6)		111.6(6)		106.6(6)		114.1(6)
OFeO bend (a)		65.6(16)		64.7(15)		53.1(12)		65.3(15)

[a] B3LYP/6-311++G(3df,3pd)/all electron level of theory. [b] Mode descriptions and symmetries. [c] Triplet pattern at 737.3, 727.1, and 714.5 cm^{-1} was observed for this mode in reaction with H_2 and $^{16}O_2 + {}^{16}O^{18}O + {}^{18}O_2$ (1:2:1).

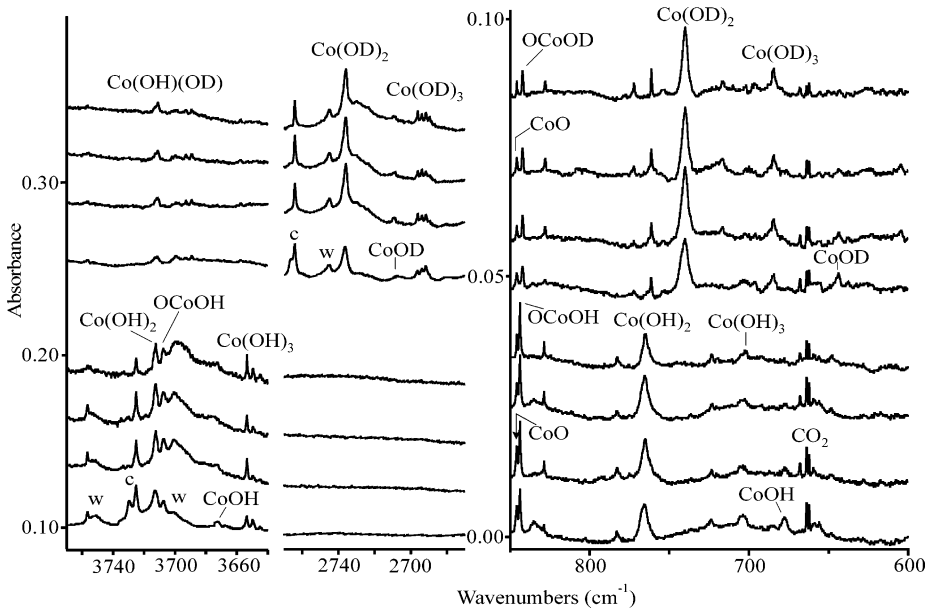

Figure 5. Infrared spectra for the cobalt atom and H_2O_2 reaction products in solid argon at 10 K. (a) Co + H_2O_2 deposition for 60 min, (b) after >290 nm irradiation, (c) after 240−380 nm irradiation, (d) after annealing to 36 K, (e) Co + D_2O_2 deposition for 60 min, (f) after >290 nm irradiation, (g) after 240−380 nm irradiation, and (h) after annealing to 36 K.

Weak additional bands were observed at 875.7 cm^{-1} for FeO and at 924.8 and 695.2 cm^{-1} for HFeOFeOH as assigned earlier, but no absorptions were found for HFeOH, the major product in water experiments.[16c]

$Co(OH)_2$. The Co atom reaction with H_2O_2 gave new absorptions at 3712.5 and 765.5 cm^{-1} (Figure 5) and a broad band centered at 496.9 cm^{-1}. These bands are located in the O−H stretching, Co−O stretching, and M−O−H bending regions, and they can be assigned to the new $Co(OH)_2$ molecule. The 765.2 cm^{-1} band is covered partly by a common H_2O_2 complex band at 766.4 cm^{-1} on deposition, but after full-arc irradiation, the complex band is wiped out. In addition, weak bands were observed for CoO_2, its dimer, and CoO, as reported earlier.[35] These bands were reproduced using $H_2 + O_2$ mixtures without overlapping the H_2O_2 complex (Figure S1), revealing the same product molecule. Weak product bands are observed on deposition, but on 240−380 nm irradiation, these bands increased markedly, and full-arc irradiation increased them even more, suggesting the formation of CoO_2 first and then further reaction with H_2 to give $Co(OH)_2$.

With D_2O_2, the O−D stretching mode shifts to 2736.1, giving the H/D 1.3569 ratio, and the Co−O stretching mode shifts slightly to 740.0 cm^{-1}. The O−D bending mode is out of our range of measurement. These bands increased on annealing (by 30%) and irradiation (by 10%) (Figure 5e−h). With $D_2 + O_2$, the same bands were observed. An experiment with $^{18}O_2$ gave substituted bands as listed in Table 3, which show the ^{18}O shifts expected for these three modes. The key observation was a triplet absorption at 765.2, 755.5, and 744.2 cm^{-1} with $H_2 + {}^{16}O_2 + {}^{16,18}O_2 + {}^{18}O_2$, indicating two equivalent oxygen atoms (Figure S1). The doublet absorptions in O−H stretching region at 3712.5 and 3710.6 cm^{-1} are very close to pure isotopic ^{16}O and ^{18}O values, suggesting that two O−H groups are involved but without coupling in this molecule.

Theoretical calculations strongly support the $Co(OH)_2$ assignment. The ground state of $Co(OH)_2$ is calculated to be ^4A with C_2 symmetry, and agreement between observed and calculated frequencies is shown in Table 3. The b symmetry antisymmetric O−H stretching mode in $Co(OH)_2$ and the same O−D stretching mode in $Co(OD)_2$ are predicted at 3912.8 and 2851.0 cm^{-1}, giving the 1.3724 H/D ratio, which is higher than the 1.3569 observed value owing to anharmonicity although both modes are overestimated by 5.1%. The Co−O stretching and O−H bending modes are predicted at 794.3 and 523.3 cm^{-1}, which are 3.8 and 5.0% higher than the experimental measurements and in the range of expected agreement.

$Ni(OH)_2$. Figure 6 a−d shows laser-ablated Ni atom reaction products with H_2O_2 in solid argon. A new band at 3712.0 cm^{-1} in the O−H stretching region, a doublet at 794.3 and 789.8 cm^{-1}, and a weak band at 510.6 cm^{-1} appeared on deposition, increased by 30% on annealing, and further increased by 20% on 240−380 nm irradiation. In addition, weak nickel oxide

TABLE 3: Observed and Calculated Frequencies (cm^{-1}) for $Co(OH)_2$ (^4A in C_2 Symmetry)[a]

	$Co(OH)_2$		$Co(OD)_2$		$Co(^{18}OH)_2$		$Co(^{18}OD)_2$	
mode[b]	obsd	calcd	obsd	calcd	obsd	calcd	obsd	calcd
OH str (a)		3915.5(1)		2853.3(1)		3902.3(1)		2834.7(0)
OH str (b)	3712.5	3913.5(219)	2736.1	2851.0(150)	3701.6	3900.4(212)	2720.1	2832.6(141)
CoO str (b)	765.5	794.6(157)	740.0	773.0(218)	744.4[c]	770.5(134)	717.7	748.7(198)
CoO str (a)		651.2(0)		616.8(0)		623.3(1)		585.6(0)
CoOH bend (b)	496.9	509.2(321)		401.5(166)	490.0	502.2(320)		394.4(164)
CoOH bend (a)		454.3(147)		349.6(5)		445.9(5)		345.0(5)
CoOH bend (a)		280.3(147)		240.1(87)		274.6(144)		233.2(84)
CoOH bend (b)		150.2(12)		136.8(11)		146.1(11)		134.0(11)
OCoO bend (a)		95.0(9)		79.1(8)		93.4(8)		78.4(8)

[a] B3LYP/6-311++G(3df,3pd)/all electron level of theory. [b] Mode descriptions and symmetries. [c] Triplet pattern at 765.5, 755.1, and 744.4 cm^{-1} was observed for this mode in reaction with H_2 and $^{16}O_2 + {}^{16}O^{18}O + {}^{18}O_2$ (1:2:1).

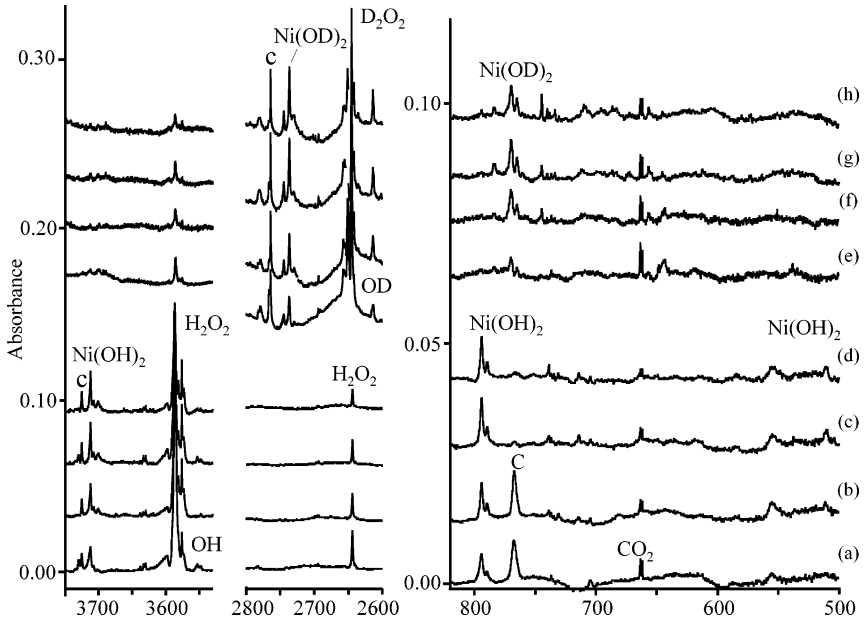

Figure 6. Infrared spectra for the nickel atom and H_2O_2 reaction products in solid argon at 10 K. (a) Ni + H_2O_2 deposition for 60 min, (b) after annealing to 20 K, (c) after >220 nm irradiation, (d) after annealing to 26 K, (e) Ni + D_2O_2 deposition for 60 min, (f) after annealing to 22 K,. (g) after >220 nm irradiation, and (h) after annealing to 26 K.

bands at 967.4 cm^{-1} ($Ni(O_2)$), 954.9 cm^{-1} (NiO_2), and 823.3 cm^{-1} (NiO)[36] were also observed as decomposition products. The analogous deuterium substituted experiment (D_2O_2) gave a new band at 2736.6 cm^{-1} and a doublet at 769.8 and 765.1 cm^{-1} (Figure 6e−h). Unfortunately, another low band shifts below our measurement region (400 cm^{-1}). As expected, weak $Ni(O_2)$ and NiO_2 bands appeared as the same as in the H_2O_2 experiment.

The doublet at 794.3 and 789.8 cm^{-1} in the H_2O_2 experiment and at 769.8 and 765.1 cm^{-1} in the D_2O_2 experiment exhibit 5:2 relative intensity for ^{58}Ni and ^{60}Ni in natural abundance, which demonstrates the participation of a single Ni atom in the new molecule.[36] A very similar frequency pattern was observed for $^{63}Cu(OH)_2$ and $^{65}Cu(OH)_2$ and $^{64}Zn(OH)_2$, $^{66}Zn(OH)_2$, and $^{68}Zn(OH)_2$ as well.[19,20]

Complementary experiments with $H_2 + O_2$ gave slightly broader bands at 3712.9 cm^{-1}, a doublet at 795.3 and 790.0 cm^{-1}, and a weak band at 511.0 cm^{-1} that correspond with H_2O_2 values very well (Figure S2). The product bands are very weak on deposition but increased 5-fold on full-arc irradiation. The slightly broader feature suggests that the escaping of H_2 on deposition left more sites in the matrix, resulting in the defect solid. The reaction with $H_2 + {}^{18}O_2$ shifted the upper band to 3700.9 cm^{-1} and the lower bands to 771.1 and 767.1 cm^{-1}, and with $D_2 + {}^{18}O_2$, these absorptions further shift to 2720.1, 747.7, and 742.5 cm^{-1}, respectively. The $H_2 + {}^{16}O_2 + {}^{16,18}O_2 + {}^{18}O_2$ reagent is used to determine the number of oxygen atoms involved in the Ni−O stretching mode, and triplet distributions at 795.3, 784.2, and 771.1 cm^{-1} (intensity 1:2:1) were observed, indicating the participation of two equivalent oxygen atoms. The doublet at 3713.0 and 3701.8 cm^{-1} is assigned to the $^{16}O-H$ and $^{18}O-H$ modes, verifying the $Ni(OH)_2$ assignment. A similar triplet at 769.8, 759.9, and 747.7 cm^{-1} and a doublet at 2737.1 and 2720.3 cm^{-1} appeared in the $D_2 + {}^{16}O_2 + {}^{16,18}O_2 + {}^{18}O_2$ experiment, further confirming the metal dihydroxide assignment.

The identification of $Ni(OH)_2$ is supported by DFT calculations, and the observed and computed frequencies are compared in Table 4. The molecular structure converges to C_{2h} symmetry in the case of Ni with linear O−Ni−O and bent Ni−O−H subunits, like that found for the coinage metal dihydroxides.[19] The ^3B_g ground state is in agreement with triplet ground states for the NiX_2 (X = F, Cl. Br, I) species.[37] The predicted Ni−O stretching frequency at 808.4 cm^{-1} and O−H bending mode at 584.6 cm^{-1} are again higher than the observed values of 794.3 and 510.6 cm^{-1}. The calculated O−H antisymmetric stretching mode at 3901.5 cm^{-1} is overestimated by 5.1%, which is consistent with the predictions for other transition metal dihydroxides.[17−20]

TABLE 4: Observed and Calculated Frequencies (cm^{-1}) for $Ni(OH)_2$ (^3B_g in C_{2h} Symmetry)[a]

	$^{58}Ni(OH)_2$		$^{58}Ni(OD)_2$		$^{58}Ni(^{18}OH)_2$		$^{58}Ni(^{18}OD)_2$		$^{60}Ni(OH)_2$	
mode[b]	Obsd	calcd	obsd	calcd	obsd	calcd	obsd	calcd	obsd	calcd
OH str (a_g)		3903.9(0)		2844.5(0)		3890.9(0)		2826.1(0)		3904.0(0)
OH str (b_u)	3712.0	3901.9(235)	2736.6	2842.1(157)	3700.9	3888.5(227)	2720.1	2823.8(148)	3712.0	3901.5(235)
NiO str (b_u)	794.3	808.3(144)	769.8	787.4(219)	771.1[c]	784.3(119)	747.7[d]	762.5(197)	789.8	803.5(141)
NiO str (a_g)		657.5(0)		622.8(0)		629.8(0)		591.2(0)		657.5(0)
NiOH bend (b_u)	510.6	584.6(337)		463.2(163)		575.9(339)		454.9(162)		584.1(338)
NiOH bend (a_u)		467.8(0)		358.0(0)		458.9(0)		353.8(0)		467.8(0)
NiOH bend (a_u)		351.9(166)		292.3(100)		346.1(163)		284.8(96)		351.6(166)
NiOH bend (b_u)		169.5(15)		154.1(14)		164.9(14)		151.1(14)		168.5(15)
ONiO bend (a_u)		113.2(4)		97.5(5)		110.9(4)		96.3(4)		112.7(4)

[a] B3LYP/6-311++G(3df,3pd)/all electron level of theory. [b] Mode descriptions and symmetries. [c] Triplet pattern at 795.3, 784.2, and 771.1 cm^{-1} was observed for this mode in reaction with H_2 and $^{16}O_2 + {}^{16}O^{18}O + {}^{18}O_2$ (1:2:1). [d] Triplet pattern at 769.8, 759.9, and 747.7 cm^{-1} was observed for this mode in reaction with D_2 and $^{16}O_2 + {}^{16}O^{18}O + {}^{18}O_2$ (1:2:1).

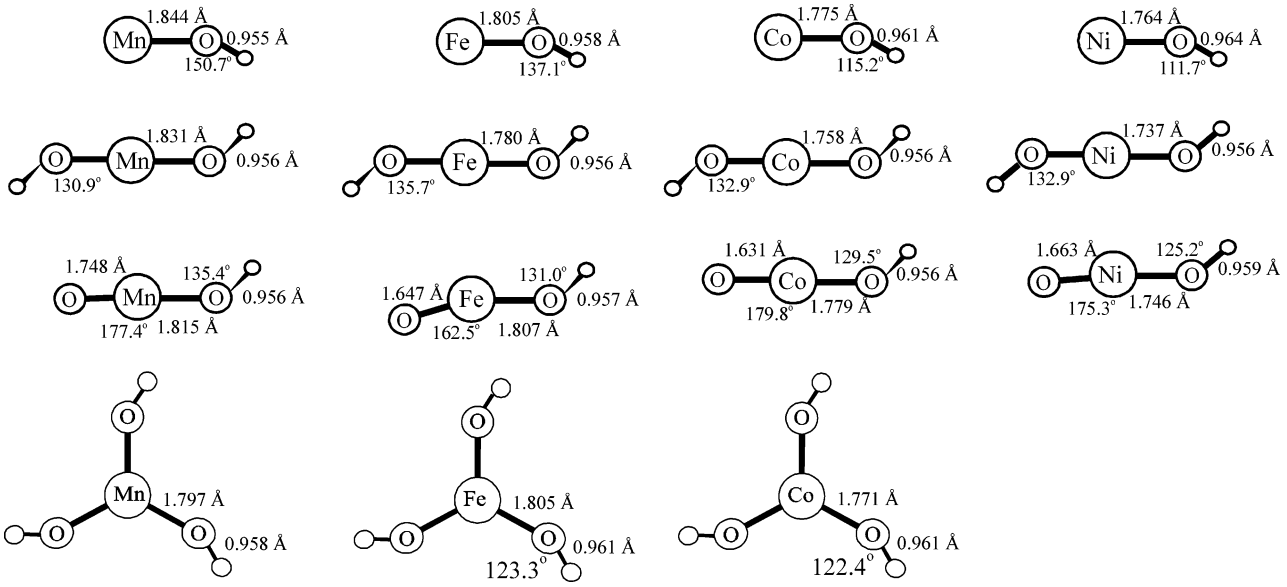

Figure 7. Structures computed for MOH [C_s symmetry], $M(OH)_2$ [C_2 for first three, C_{2h} for Ni], OMOH [C_s], and $M(OH)_3$ [C_s for Mn and C_{3h} for Fe and Co) at the B3LYP/6-311++G(3df,3pd)/SDD level of theory.

Trihydroxides ($M(OH)_3$). Sharp new absorptions were observed at 3674.8 and 3665.1 cm^{-1} in the upper region and at 723.1 cm^{-1} in the lower region in iron and hydrogen peroxide experiments. These bands increase slightly on full-arc irradiation, and they increase together relative to $Fe(OH)_2$ in H_2O_2 experiments using higher laser energy. Counterparts were observed with D_2O_2 at 2709.8 and 2704.4 cm^{-1} and at 701.3 cm^{-1}. The former exhibit the H/D ratios 1.357 and 1.355 for an O−H stretching mode and fall 53−62 cm^{-1} below this mode for $Fe(OH)_2$, and the latter is 14.2 cm^{-1} below the Fe−O stretching mode for $Fe(OH)_2$. Hence, another iron hydroxide molecule is expected. The monohydroxide is calculated to absorb weakly 35 cm^{-1} below the dihydroxide, the trihydroxide is predicted to have strong degenerate stretching modes 50 and 29 cm^{-1} below the corresponding modes for $Fe(OH)_2$, and the tetrahydroxide is computed to absorb strongly 112 cm^{-1} lower than the dihydroxide. The new bands are in good agreement with frequency shifts computed for the $Fe(OH)_3$ molecule, relative to the $Fe(OH)_2$ molecule, and they are assigned accordingly. The observed 21.8 cm^{-1} deuterium shift for the Fe−O stretching mode is in good agreement with the calculated 20.9 cm^{-1} value. The $Fe(OH)_3$ molecule is formed by further reaction of $Fe(OH)_2$ with H_2O_2 during sample deposition.

Computations at the B3LYP level did not locate a quartet state but converged to a stable $^6A'$ state ($<s^2> = 8.76$) for $Fe(OH)_3$ in C_{3h} symmetry. The structure is compared with those for other iron hydroxide molecules in Figure 7. The OH and Fe−O stretching modes of $Fe(OH)_3$ are predicted at 3866.2 and 714.1 cm^{-1}, respectively, which match the experimental data very well.

New absorptions appeared at 3649.7, 702.8, and 570.3 cm^{-1} with cobalt and H_2O_2 and shifted to 2691.7, 683.9, and 430.5 cm^{-1} with D_2O_2. Again, these bands were favored relative to the dihydroxide using higher laser energy, which helps to promote further reaction, and they are observed 62.9 and 42.0 cm^{-1} below the O−H and Co−O stretching modes for $Co(OH)_2$. Our B3LYP calculations predict these modes for CoOH to fall 53 and 156 cm^{-1} lower, for $Co(OH)_3$ to fall 42 and 71 cm^{-1} lower, and for $Co(OH)_4$ to appear 119 and 92 cm^{-1} lower, respectively. Good agreement is found for the trihydroxide observations, and these bands are assigned accordingly.

Our calculations for $Co(OH)_3$ converged to a $^5A'$ state ($<s^2> = 6.02$) in C_{3h} symmetry with all real frequencies, and the triplet state failed to converge. The structure is illustrated in Figure 7, and the degenerate e′ stretching modes were calculated at 3858 and 715 cm^{-1}.

No absorptions are observed for $Mn(OH)_3$ and $Ni(OH)_3$. The former calculation gave a C_s structure and strong infrared absorptions at 3899, 720, and 682 cm^{-1}, and the latter calculation failed to converge.

Metal Oxyhydroxides (OMOH). A group of new bands at 3707.4, 844.2, and 464.6 cm^{-1} was observed with Co in H_2O_2 and the hydrogen/oxygen mixture experiments. With ^{18}O substitution, these bands shift to 3695.4, 812.1, and 460.1 cm^{-1},

TABLE 5: Observed and Calculated Frequencies (cm^{-1}) for MOH (M = Ni, Co, Fe, Mn)[a]

	NiOH[^{2}A″]		NiOD		CoOH[^{3}X]		CoOD	
mode	obsd	calcd	obsd	calcd	obsd	calcd	obsd	calcd
OH str (a)		3808.1(45)		2771.2(31)	3672.2	3862.8(65)	2709.4	2813.8(45)
MO str (a)[b]	704.7	749.5(105)	642.9	657.5(114)	677.2?	707.5(70)	655.5?	689.7(96)
OH bend (a)[b]		645.1(55)		534.0(20)		450.5(134)		337.9(65)
	FeOH[^{6}A″]		FeOD		MnOH[^{7}A]		MnOD	
mode	obsd	calcd	obsd	calcd	obsd	calcd	obsd	calcd
OH str. (a)		3893.5(54)		2836.6(42)	3654.2	3923.7(40)	2693.9	2859.4(37)
MO str. (a)		679.2(100)		661.1(119)	631.1	649.7(133)	606.1	631.9(139)
OH bend (a)		352.0(120)		264.2(62)		193.2(124)		144.8(70)

[a] B3LYP/6-311++G(3df,3pd)/all electron level of theory. The triplet ground state of Co(OH) is not defined. [b] Mode descriptions and symmetries. The M−O stretching and M−O−H bending modes mix in these planar molecules, and based on the H to D shift, much more mode mixing occurs in NiOH than the other MOH cases shown here.

respectively. The 844.2 cm^{-1} band defines a 1.0395 $^{16}O/^{18}O$ frequency ratio that is appropriate for the Co−O stretching mode although the ratio is slightly lower than most of the Co−O modes in cobalt oxides.[35] The 3707.4 cm^{-1} band is due to the O−H stretching mode defining the 1.0032 $^{16}O/^{18}O$ ratio, and the 460.1 cm^{-1} band is located in the OH bending region. The scrambled oxygen isotopic experiment gave a doublet (3707.4 and 3695.4 cm^{-1}) for the OH stretching mode, a quartet (844.2, 841.3, 816.8, and 812.1 cm^{-1}) for the Co−O stretching mode (shown in Figure S1), and a broad band feature for the OH bending mode. With D_2O_2 or $D_2 + O_2$, the Co−O stretching mode shifts to 842.5 cm^{-1}, and the O−D stretching is overlapped by the O−D band of $Co(OD)_2$. Noting the diagnostic isotopic distribution for the Co−O stretching mode suggests that the mode is perturbed by the OH subunit, which is the 1.7 cm^{-1} D-shift, 2.9 cm^{-1} red-shift when the Co−O mode was perturbed by ^{18}O, and the 4.7 cm^{-1} blue-shift when the Co-^{18}O mode is perturbed by ^{16}O. Calculations were done for the trihydroxide dehyration product HOCoO and a $^5A'$ ground-state converged in C_s symmetry with a strong terminal Co−O mode at 861.5 cm^{-1}, O−H stretching mode at 3911.9 cm^{-1}, and O−H bending mode at 493.8 cm^{-1}, which are in good agreement with experimental results. The deuterium shift of 0.5 cm^{-1}, 16:18 ratio 1.0413, and 16−18 mixture pattern match the observed bands very well, which strongly support this assignment. Similar molecules OMOH (M = Sc, Y, La) have been identified in our early reports.[17]

The OFeOH species was trapped in H_2O_2 and hydrogen/oxygen mixture experiments, which is analogous to OCoOH. A group of new absorptions at 3719.4, 873.1, and 456.9 cm^{-1} appeared on deposition and increased on 240−380 nm irradiation and annealing. With ^{18}O, these bands shift to 3707.7, 839.0, and 453.1 cm^{-1}, respectively, which are appropriate to OH stretching, Fe−O stretching, and OH bending modes. The 873.1 cm^{-1} band is very close to diatomic FeO stretching frequency but with ^{18}O substitution, two bands separated totally as shown in Figure 4. With D_2O_2 or $D_2 + O_2$, the Fe−O stretching mode shifts red only 0.5 cm^{-1}, the O−H stretching mode to 2742.1 cm^{-1}, and the O−H bending mode is out of our measurement. With the scrambled oxygen sample quartet pattern for the Fe−O mode, doublet pattern for the O−H mode, and the unresolved triplet for the OH bending mode suggest OFeOH assignment. Accordingly, we assigned this group of bands to OFeOH. The assignment is strongly supported by our DFT frequency calculation, which converged to a sextet state with a planar structure. The strong frequencies of OFeOH predicted at 3917.7 cm^{-1} (OH str), 900.1 cm^{-1} (Fe−O str), and 473.8 cm^{-1} (OH bend) are overestimated by 5.3, 3.1, and 3.5%, respectively, which are in very good consistency. Diagnostic information is also obtained for the Fe−O mode from mixed ^{16}O, ^{18}O substitution, and the calculated quartet at 900.1, 898.8, 866.1, and 863.3 cm^{-1} match observed values very well.

There are no absorptions observed for OMnOH and ONiOH in our experiments, suggesting that OMOH is generated from metal trihydroxides, which are dehydrated to give oxyhydrides. As shown in our experiments, neither $Mn(OH)_3$ nor $Ni(OH)_3$ was obtained.

Monohydroxides (MOH). Laser-ablated metal atom reactions with H_2O_2 can also give MOH molecules from decomposition of the energized $M(OH)_2$ primary product (M = Ni, Co, Fe, and Mn), and weak bands can be expected for M−O and O−H stretching modes. New weak bands at 704.7 cm^{-1} in H_2O_2 and 642.9 cm^{-1} in D_2O_2 experiments appeared on deposition with Ni, decreased on annealing to 20 K, and further decreased on 240−380 nm irradiation, which are appropriate for NiOH and NiOD, respectively. Our frequency calculations for NiOH at 749.5 cm^{-1} and NiOD at 657.5 cm^{-1} support the assignment of the previous weak bands. However, there was no such band observed in $O_2 + H_2$ experiments, so these bands cannot be confirmed by ^{18}O substitution.

In Co + H_2O_2 experiments, a weak band at 702.5 cm^{-1} (Co−O stretching region) and 3672.2 cm^{-1} (O−H stretching region) appeared on deposition, decreased on annealing but increased on 240−380 nm irradiation. The deuterium counterpart is found at 684.6 and 2709.4 cm^{-1} in the D_2O_2 experiment. These bands are assigned to CoOH and CoOD, respectively. Our DFT calculation predicts the Co−O and O−H stretching modes of triplet ground-state CoOH at 707.5 and 3862.8 cm^{-1} and the same modes of CoOD at 689.7 and 2813.8 cm^{-1}, which match the experimental values very well. Our calculations predict this mode 50 cm^{-1} below the corresponding mode for the dihydroxide, and the previous band is 40 cm^{-1} lower. No Fe−O stretching mode absorption was observed for FeOH, which is predicted at 679.2 cm^{-1} some 113 cm^{-1} below the dihydroxide.

A weak band observed at 631.1 cm^{-1} tracks a 3654.2 cm^{-1} band in the Mn + H_2O_2 experiment, and these are appropriate for Mn−O and O−H stretching modes of MnOH. The deuterium counterpart appeared at 606.1 and 2693.9 cm^{-1}. The B3LYP calculation predicts MnOH to have a septet ground-state and a quintet-state lies 6.0 kcal/mol higher. The calculated Mn−O and O−H stretching modes of MnOH at 649.7 and 3923.7 cm^{-1} and the same modes of MnOD at 631.9 and 2859.4 cm^{-1} are within the error of transition metal hydroxide calculations.

Reaction Mechanisms. The stable $M(OH)_2$ molecules are produced through energized metal atom reactions with H_2O_2

TABLE 6: Observed and Calculated Frequencies (cm^{-1}) for $M(OH)_3$ (M = Fe, Co) in C_{3h} Symmetry[a]

	$Fe(OH)_3[^6A]$		$Fe(OD)_3$		$Co(OH)_3[^5A]$		$Co(OD)_3$	
mode[b]	calcd	obsd	calcd	obsd	calcd	obsd	calcd	obsd
OH str (a)	3869.7(0)		2818.4(0)		3862.6(1)		2813.1(1)	
OH str (e)	3866.2(163 2)	3674.8 3665.1	2815.0(1062)	2709.8 2704.4	3857.9(2122)	3649.7	2808.8(1342)	2691.7
MO str (e)	714.1(105 2)	723.1	693.2(1732)	701.3	714.8(672)	702.8	689.9(1542)	683.9
MO str (a)	639.5 (0)		623.6(0)		645.1(0)		630.3(0)	
OH bend (e)	605.0(216 2)		466.9(842)		607.8(2242)	570.3	472.4(972)	430.5
OH bend (a)	600.2(0)		444.2(0)		598.2(0)		443.1(0)	

[a] B3LYP/6-311++G(3df,3pd)/all electron level of theory. [b] Only OH and MO stretching and OH bending modes are listed: the lower modes for Fe are 383.0(339), 371.1(0 × 2), 149.6(10 × 2), and 142.1(5) and for Co are 294.1(289), 265.0(0), 159.2(26 × 2), and 152.0(10).

TABLE 7: Observed and Calculated Frequencies (cm^{-1}) for OM(OH) (M = Ni, Co, Fe, Mn)[a]

	$OFe(OH)[^5A]$		$OFe(OD)$		$OMn(OH)[^6A]$	$OMn(OD)$
mode[b]	calcd	obsd	calcd	obsd	calcd	calcd
OH str (a)	3917.7(125)	3719.4	2853.8(85)	2742.1	3889.4(134)	2832.5(88)
MO str (a)	900.1(129)	873.1	899.6(130)	872.6	824.8(102)	823.5(107)
M−OH str (a)	667.1(44)		646.4(73)		686.0(42)	656.4(86)
OH bend (a)	473.8(185)	456.9	360.2(101)		586.4(156)	458.8(68)
OH bend (a)	137.0(59)		109.3(150)		195.7(103)	115.1(39)
OMO bend (a)	115.1(33)		77.3(37)		108.4(29)	107.4(27)
	$OCo(OH)[^5A]$		$OCo(OD)$		$ONi(OH)[^4A]$	$ONi(OD)$
mode	calcd	obsd	calcd	obsd	calcd	calcd
OH str (a)	3911.9(123)	3707.4	2849.5(84)		3882.8(114)	2827.6(76)
MO str (a)	862.8(103)	844.2	862.3(100)	842.5	480.6(19)	449.8(57)
M−OH str (a)	673.5(33)		653.6(67)		726.1(102)	719.0(131)
OH bend (a)	493.8(191)	464.6	374.1(101)		644.5(135)	515.2(16)
OH bend (a)	137.0(59)		137.1(60)		179.5(22)	172.9(21)
OMO bend (a)	115.1(33)		112.0(31)		158.7(159)	152.4(16)

[a] B3LYP/6-311++G(3df,3pd)/all electron level of theory. [b] Mode descriptions and symmetries for C_s molecules.

TABLE 8: Structures, Charges, and Reaction Energies Calculated for First Row Transition Metal $M(OH)_2$ Molecules[a]

molecule	state, symmetry	M−O (Å)	O−H (Å)	O−M−O (deg)	M−O−H (deg)	Mulliken charge q(M)	Mulliken charge q(O)	Mulliken charge q(H)	natural charge q(M)	natural charge q(O)	natural charge q(H)	ΔE (kcal/mol)
$Sc(OH)_2$[b]	$^2A_1$, C_{2v}	1.936	0.953	172.2	177.7	0.850	−1.00 6	0.581	1.343	−1.15 8	0.487	−185
$Ti(OH)_2$[c]	$^3B_1$, C_{2v}	1.828	0.958	172.7	180.0	1.008	−1.15 9	0.480	1.275	−1.12 4	0.487	−182
$V(OH)_2$[d]	^4B, C_2	1.789	0.953	180.0	180.0	0.885	−1.08 5	0.643	1.191	−1.08 4	0.488	−177
$Cr(OH)_2$[d]	$^5A_1$, C_{2v}	1.817	0.958	172.7	133.1	0.891	−0.92 5	0.480	1.282	−1.11 1	0.470	−129
$Mn(OH)_2$	^6A, C_2	1.831	0.957	180.0	132.1	0.955	−0.93 9	0.462	1.494	−1.21 8	0.471	−162
$Fe(OH)_2$	^5A, C_2	1.780	0.956	179.9	135.7	0.839	−0.90 4	0.419	1.373	−1.16 5	0.479	−124
$Co(OH)_2$	^4A, C_2	1.758	0.956	177.9	132.9	0.815	−0.88 2	0.475	1.344	−1.14 7	0.475	−152
$Ni(OH)_2$	^3B_g, C_{2h}	1.737	0.957	180.0	130.1	0.779	−0.85 6	0.467	1.286	−1.11 6	0.473	−116
$Cu(OH)_2$[e]	^2B_g, C_{2h}	1.753	0.963	180.0	117.1	0.569	−0.73 6	0.451	1.172	−1.04 5	0.459	−86
$Zn(OH)_2$[f]	^1A, C_2	1.774	0.960	173.9	115.5	0.782	−0.82 4	0.433	1.559	−1.23 9	0.460	−86

[a] B3LYP/6-311++G(3df,3pd)/all electron level of theory. [b] Ref 17. [c] Ref 18. [d] Refs 41 and 42. [e] Ref 19. [f] Ref 20.

and trapped in solid argon (reaction 1), and the calculated exothermic reaction energies are listed in Table 8.

The Sc atom reaction with H_2O_2 is the most exothermic, and this exothermicity decreases from Sc to Zn, indicating that the amount of electron transfer is decreased, which is consistent with the pattern of observed O−H stretching frequencies.

$$M + H_2O_2 \rightarrow [M(OH)_2]^* \xrightarrow{\text{relax}} M(OH)_2 \quad (1)$$

The $M(OH)_2$ molecule can also be obtained through a metal reaction with the $O_2 + H_2$ mixture, and this reaction 2 appears to form the [OMO*] intermediate, which then reacts with H_2.

$$M + O_2 + H_2 \rightarrow [OMO^*] + H_2 \rightarrow M(OH)_2 \quad (2)$$

The small yield of MOH is generated from decomposition of the energized $[M(OH)_2]^*$ intermediate first formed in reaction 1 before it can be relaxed by the cold matrix, reaction 3. Also, the dihydroxide molecules can react further with H_2O_2 to form trihydroxides and tetrahydroxides. Reaction 4 is exothermic by 11, 13, 34, and 47 kcal/mol for Mn, Fe, Co, and Ni, respectively. Reaction 5 is exothermic by 32 kcal/mol for Mn, 49 kcal/mol for Fe, and 59 kcal/mol for Co.

$$[M(OH)_2]^* \rightarrow MOH + OH \quad (3)$$

$$M(OH)_2 + H_2O_2 \rightarrow M(OH)_3 + OH \quad (4)$$

$$M(OH)_2 + H_2O_2 \rightarrow M(OH)_4 \quad (5)$$

The $M(OH)_3$ and $M(OH)_4$ molecules are apparently dehydrated to give metal oxyhydroxides or metal oxides.

$$M(OH)_3 \rightarrow OMOH + H_2O \quad (6)$$

$$M(OH)_4 \rightarrow MO_2 + 2H_2O \quad (7)$$

Bonding Character for Transition Metal Dihydroxides. The transition metal dihydroxide molecules can be viewed as similar to the transition metal dihalide molecules. Most experi-

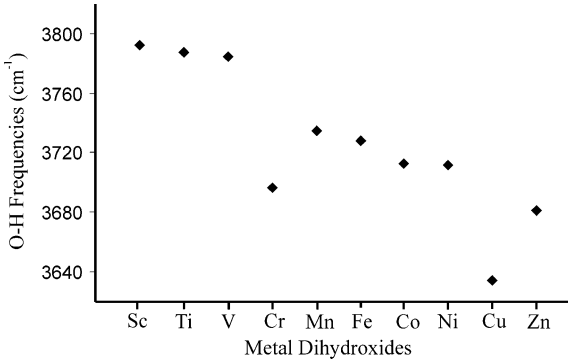

Figure 8. Correlation of the O−H stretching frequencies for the first row transition metal dihydroxide molecules.

ments and theoretical calculations agree on linear or quasi-linear structures for the first row transition metal dihalides, which can be rationalized by 3d−4s hybridization with maximum electron density in a plane perpendicular to the molecular axis that stabilizes the linear structure.[37] As is shown in Table 8, a similar quasi-linear O−M−O skeleton is obtained for the first row transition metal dihydroxide molecules. However, the M−O−H bond angle is decreased from Sc−O−H (quasi-linear) to Zn−O−H (bent), giving some new bonding information between the metal and the OH ligand. The Mulliken and natural charge distributions are listed in the same table. It is also interesting to compare the strong antisymmetric OH stretching frequency, which steadily red-shifts from $Sc(OH)_2$ to $Zn(OH)_2$, but this frequency for Cr and Cu is exceptionally low as is shown in Figure 8.

Since (n − 1)d orbitals are lower in energy than the ns orbitals, the interaction between electronegative ligands and ns orbitals plays a very important role. As we already know, for most of neutral first row transition metals, the ground-state electron configuration is [core]$3d^n4s^2$, but Cr and Cu have half-filled and filled d shells and $3d^54s^1$ and $3d^{10}4s^1$ valence electron configurations, respectively.[40] One can therefore expect minimum repulsive interaction between ligands and Cr or Cu, which matches what we observed for the O−H stretching frequencies for first row transition metal dihydroxide molecules,[17−20,41,42] where $Cr(OH)_2$ and $Cu(OH)_2$ do exhibit exceptionally low O−H stretching frequencies. The low OH stretching frequencies for $Cr(OH)_2$ and $Cu(OH)_2$ reflect more OH electron pair donation to the metal centers, suggesting that these two metal centers have less electron distributions on 4s orbitals and that other metals have similar higher 4s electron distributions. However, for the first row M^+, the 4s orbitals are empty. If the metal center is charged +1 for $M(OH)_2$, the O−H stretching frequencies of the V^+, Cr^+, Co^+, Ni^+, and Cu^+ centers are lower since 4s orbitals of these metal cations are empty.[40] However, this is not the case in our experiment. For first row M^{2+}, the 4s orbitals of all metals are empty. On the basis of this result, we can conclude that the charges of metal centers for first row metal dihydroxide molecules are less than +1 and that the calculated Mulliken charges are more reasonable than the natural charges.

The M−O−H bond angles reflect the covalent bond character. On the basis of VSEPR theory (valence-shell electron-pair repulsion), the M−O−H angles depend on two lone pairs of electrons around the oxygen atom. The bent M−O−H bond has been found for group 11 and 12 metal dihydroxides, and the 111.1° angle in Au−O−H in $Au(OH)_2$ and 109.1° of Hg−O−H in $Hg(OH)_2$ are only 6.6 and 4.6° higher than the H_2O bond angle, which is amazing for these metal hydroxides to have so strong a covalent character. In contrast, for early transition metal dihydroxides, the more electronegative oxygen averages the repulsion of two lone pair electrons, and the molecules favor linear structures. The heavy alkaline earth metal hydroxides have similar structures with nearly linear M−O−H linkages.[43]

Conclusion

Laser-ablated transition metal Mn, Fe, Co, and Ni atom reactions with H_2O_2 or $H_2 + O_2$ mixtures gave the metal dihydroxide molecules $M(OH)_2$ as major products, which were identified by deuterium and ^{18}O isotopic substitution and DFT frequency calculations. Decomposition of the dihydroxide can occur, and evidence is presented for Co(OH) and Ni(OH) in solid argon. Further reaction with H_2O_2 leads to trihydroxide molecules, and we have evidence for $Fe(OH)_3$ and $Co(OH)_3$, which are dehydrated to give metal oxyhydroxide, OFeOH, and OCoOH molecules. The first row transition metal dihydroxide molecules exhibit a smoothly decreasing trend for the antisymmetric O−H stretching frequency with the exception of Cr and Cu, which are lower due to different s−d orbital populations and more covalent character.

Acknowledgment. We gratefully acknowledge financial support for this research from NSF Grant CHE 03-52487.

Supporting Information Available: Figures showing infrared spectra for the cobalt atom and nickel atom reaction products S1 and S2. This material is available free of charge via the Internet at http://pubs.acs.org.

References and Notes

(1) Cotton, F.; Wilkinson, G.; Murillo, C. A.; Bochmann, M. *Advanced Inorganic Chemistry*, 6th ed.; Wiley: New York, 1999.

(2) Wells, A. F. *Structural Inorganic Chemistry*, 4th ed.; Clarendon Press: Oxford, 1975. (b) See also the Inorganic Crystal Structure Database.

(3) Schubert, K.; Seitz, A. *Ziet. Anorg. Chem.* **1948**, *256*, 226.

(4) Christensen, A. N. *Acta Chem. Scand.* **1965**, *19*, 1765.

(5) Shieh, S. R.; Duffy, T. S. *Phys. Rev. B* **2002**, *66*, 134301.

(6) Watanabe, K.; Kikuoka, T.; Kumagai, N. *J. Appl. Electrochem.* **1995**, *25*, 219.

(7) Dinamani, M.; Kamath, P. V. *J. Appl. Electrochem.* **2000**, *305*, 1157.

(8) Hou, Y.; Kondoh, H.; Shimojo, M.; Kogure, T.; Ohta, T. *J. Phys. Chem. B* **2005**, *109*, 19094.

(9) Maheswari, S. U.; Kalaignan, G. P.; Vasudevan, T. *Bull. Electrochem.* **2005**, *21*, 49.

(10) (a) Ben Salah, M.; Vilminot, S.; Andre, G.; Bouree-Vigneron, F.; Richard-Plouet, M.; Mhiri, T.; Kurmoo. M. *Chem. Mater.* **2005**, *17*, 2612. (b) Ben Salah, M.; Vilminot, S.; Andre, G.; Richard-Plouet, M.; Bouree-Vigneron, F.; Mhiri, T.; Kurmoo. M. *Chem.—Eur. J.* **2004**, *10*, 2048. (c) Ben Salah, M.; Vilminot, S.; Mhiri, T.; Kurmoo. M. *Eur. J. Inorg. Chem.* **2004**, 2272. (d) Vilminot, S.; Richard-Plouet, M.; Andre, G.; Swierczynski, D.; Bouree-Vigneron, F.; Kurmoo, M. *Inorg. Chem.* **2003**, *42*, 6859.

(11) (a) Bergquist, C.; Fillebeen, T.; Morlok, M. M.; Parkin, G. *J. Am. Chem. Soc.* **2003**, *125*, 6189. (b) Ebitani, K.; Motokura, K.; Mizugaki, T.; Kaneda, K. *Ang. Chem., Int. Ed.* **2005**, *44*, 3423. (c) Mori, K.; Kara, T.; Mizugaki, T.; Ebitani, K.; Kaneda, K. *J. Am. Chem. Soc.* **2004**, *126*, 10657. (d) Mori, K.; Kara, T.; Mizugaki, T.; Ebitani, K.; Kaneda, K. *J. Am. Chem. Soc.* **2003**, *125*, 11460.

(12) Trkula, M.; Harris, D. O. *J. Chem. Phys.* **1983**, *79*, 1138.

(13) Jarman, C. N.; Fernando, W. T. M. L.; Bernath, P. F. *J. Mol. Spectrosc.* **1990**, *144*, 286. (b) Ibid, **1991**, *145*, 151.

(14) Whitham, C. J.; Ozeki, H.; Saito, S. *J. Chem. Phys.* **2000**, *112*, 641.

(15) Schroder, D.; Schwarz, H. *Int. J. Mass Spectrosc.* **2003**, *227*, 121.

(16) (a) Zhang, L.; Dong, J.; Zhou, M. *J. Phys. Chem. A* **2000**, *104*, 8882. (b) Zhou, M.; Zhang, L. N.; Dong, J.; Quin, Q. Z. *J. Am. Chem. Soc.* **2000**, *122*, 10680; ibid, **2001**, *123*, 135 (Ti, V + H_2O). (c) Zhang, L.; Zhou, M.; Shao, L.; Wang, W.; Fan, K.; Qin, Q. *J. Phys. Chem.* **2001**, *105*, 6998 (Fe + H_2O). (d) Zhou, M.; Zhang, L. N.; Shao, L. M.; Wang, W. N.; Fan, K. N.; Qin, Q. Z. *J. Phys. Chem. A* **2001**, *105*, 5801 (Mn + H_2O). (e) Kauffman, J. W.; Hauge, R. H.; Margrave, J. L. *J. Phys. Chem.* **1985**, *89*,

3541 (Cr−Zn + H_2O). (f) Kauffman, J. W.; Hauge, R. H.; Margrave, J. L. *J. Phys. Chem*. **1985**, *89*, 3547 (Sc, Ti, V + H_2O).

(17) Wang, X.; Andrews, L. *J. Phys. Chem. A* **2006**, *110*, 1850 (Sc + H_2O_2).

(18) (a) Wang, X.; Andrews, L. *Inorg. Chem*. **2005**, *44*, 7189. (b) Wang, X.; Andrews, L. *J. Phys. Chem. A* **2005**, *109*, 10689 (Group 4 + H_2O_2).

(19) Wang, X.; Andrews, L. *Inorg. Chem.* **2005**, *44*, (Cu, Ag, Au + H_2O_2).

(20) Wang, X.; Andrews, L. *J. Phys. Chem. A* **2005**, *109*, 3849 (Zn, Cd, Hg + H_2O_2).

(21) Andrews, L. *Chem. Soc. Rev***. 2004**, *33*, 123.

(22) Andrews, L.; Citra, A. *Chem. Rev*. **2002**, *102*, 885.

(23) Wang, X.; Andrews, L. *J. Phys. Chem. A* **2003**, *107*, 4081.

(24) Pettersson, M.; Tuominen, S.; Rasanen, M. *J. Phys. Chem. A* **1997**, *101*, 1166.

(25) Pehkonen, S.; Pettersson, M.; Lundell, J.; Khriachtchev, L.; Rasanen, M. *J. Phys. Chem. A* **1998**, *102*, 7643.

(26) Frisch, M. J.; Trucks, G. W.; Schlegel, H. B.; Scuseria, G. E.; Robb, M. A.; Cheeseman, J. R.; Zakrzewski, V. G.; Montgomery, J. A., Jr.; Stratmann, R. E.; Burant, J. C.; Dapprich, S.; Millam, J. M.; Daniels, A. D.; Kudin, K. N.; Strain, M. C.; Farkas, O.; Tomasi, J.; Barone, V.; Cossi, M.; Cammi, R.; Mennucci, B.; Pomelli, C.; Adamo, C.; Clifford, S.; Ochterski, J.; Petersson, G. A.; Ayala, P. Y.; Cui, Q.; Morokuma, K.; Malick, D. K.; Rabuck, A. D.; Raghavachari, K.; Foresman, J. B.; Cioslowski, J.; Ortiz, J. V.; Stefanov, B. B.; Liu, G.; Liashenko, A.; Piskorz, P.; Komaromi, I.; Gomperts, R.; Martin, R. L.; Fox, D. J.; Keith, T.; Al-Laham, M. A.; Peng, C. Y.; Nanayakkara, A.; Gonzalez, C.; Challacombe, M.; Gill, P. M. W.; Johnson, B.; Chen, W.; Wong, M. W.; Andres, J. L.; Gonzalez, C.; Head-Gordon, M.; Replogle, E. S.; Pople, J. A. *Gaussian 98*, Revision A.6; Gaussian, Inc.: Pittsburgh, PA.

(27) Frisch, M. J.; Pople, J. A.; Binkley, J. S. *J. Chem. Phys.* **1984**, *80*, 3265 and references therein.

(28) Andrae, D.; Haeussermann, U.; Dolg, M.; Stoll, H.; Preuss, H. *Theor. Chim. Acta* **1990**, *77*, 123.

(29) Wang, X.; Andrews, L. *J. Phys. Chem. A* **2001**, *105*, 5812.

(30) Zhou, M.; Hacalogu, J.; Andrews, L. *J. Chem. Phys*. **1999**, *110*, 9450.

(31) Milligan, D. E.; Jacox, M. E. *J. Mol. Spectrosc*. **1973**, *46*, 460.

(32) Jacox, M. E.; Thompson, W. E. *J. Chem. Phys*. **1994**, *100*, 750.

(33) Chertihin, G. V.; Andrews, L. *J. Phys. Chem. A* **1997**, *101*, 8547 (Mn + O_2).

(34) Chertihin, G. V.; Saffel, W.; Yustein, J. T.; Andrews, L.; Neurock, M.; Ricca, A.; Bauschlicher, C. W., Jr. *J. Phys. Chem.* **1996**, *100*, 5261 (Fe + O_2).

(35) Chertihin, G. V.; Citra, A.; Andrews, L.; Bauschlicher, C. W., Jr. *J. Phys. Chem. A* **1997**, *101*, 8793 (Co + O_2).

(36) (a) Citra, A.; Chertihin, G. V.; Andrews, L.; Neurock, M. *J. Phys. Chem. A* **1997**, *101*, 3109. (b) Danset, D.; Manceron, L.; Andrews, L. *J. Phys. Chem. A* **2001**, *105*, 7205 (Ni + O_2).

(37) (a) Hargittai, M. *Chem. Rev*. **2000**, *100*, 2233. (b) Kaupp, M. *Angew. Chem., Int. Ed.* **2001**, *40*, 3534.

(38) Scott, A. P.; Radom, L. *J. Phys. Chem.* **1996**, *100*, 16502.

(39) Kellogg, C. B.; Irikura, K. K. *J. Phys. Chem. A* **1999**, *103*, 1150.

(40) Moore, C. E. *Atomic Energy Levels*; National Bureau of Standards, Circular 467: Washington, DC, 1952.

(41) Wang, X.; Andrews, L., in preparation (V, Nb, Ta + H_2O_2).

(42) Wang, X.; Andrews, L. *J. Phys. Chem. A*, in press.

(43) Wang, X.; Andrews, L. *J. Phys. Chem. A* **2005**, *109*, 2782 (Group 2 + H_2O_2).